Journal of Molecular Modeling (2026) 32:43
https://doi.org/10.1007/s00894-025-06593-4

RESEARCH

Bistable carbon nanobracelets

Sergey A. Vyrko[1] · Yulia G. Polynskaya[2] · Nikita A. Matsokin[2] · Andrey M. Popov[3] · Andrey A. Knizhnik[2] · Sergey V. Ratkevich[1] · Nikolai A. Poklonski[1]

Received: 11 September 2025 / Accepted: 25 November 2025

Abstract

Context Existence of bistability for carbon nanobracelets (cyclic molecules with alternating polycyclic regions and double carbon chains) is predicted using calculations based on density functional theory (DFT). It was found that two stable states have the same topological structure of covalent bonds, but different symmetries, with the total energy of the low-symmetry state lower by 1.0 and 0.8 eV than the energy of the high-symmetry state for the nanobracelets consisting of 4 and 5 monomers, respectively. On the basis of the calculated structural characteristics and electronic properties, we propose that the bistability of the carbon nanobracelets is related to the competition between the electron structure energy and the energy of interaction between the adjacent chains.

Methods Structure optimization of carbon nanobracelets was performed using spin-polarized all-electron DFT calculations with the PBE functional implemented in the Priroda code. Due to chain flexibility, a multi-step procedure was employed. The initial coordinates, derived from molecular mechanics and hand-made designs, were refined via PM3 (MOPAC2016) to generate starting points for high- and low-symmetry states. The final optimization was performed in the Priroda code without symmetry restrictions. Energies included zero-point corrections. Extended triple-n Gaussian basis sets, with kinetically balanced small components, were employed. Molecular symmetry was determined using WebMO algorithms. Positive vibrational frequencies confirmed true energy minima. The GFN-xTB method with van der Waals correction D4 was used to verify DFT-PBE calculations. To investigate the stability of the local minima, we performed *ab initio* molecular dynamics simulations. The molecular electrostatic potential was visualized using Jmol.

Keywords Bistable molecule · Carbyne · Bistability · Carbon chain · Cyclic polymer

Introduction

Bistable molecules have found wide applications in magnetic [1–5], electronic [1, 6–8], and optical [9, 10] sensors and devices. Recent advances in molecule-based systems have enabled light- or electrical-induced switching between different spin or electronic states, opening pathways for integration into memory and electronic devices [1, 2, 6–8]. For example, bistable carbene systems can be switched between singlet and triplet states via light irradiation, which holds promise for information storage applications [1]. Nanographenes and diradicaloid systems with tunable open- and closed-shell states also show potential in molecular electronics [2, 3, 6, 7], while switchable molecules integrated into microelectromechanical systems have shown high sensitivity to external stimuli, serving as molecular-scale sensors [4]. Recent studies have demonstrated that Co-based complexes can undergo ultrafast photoinduced spin-state transitions, enabling optical control over magnetization on the femtosecond timescale [9, 10]. This phenomenon opens new possibilities for integrating light-responsive single molecule magnets (SMMs) into future spintronic and photonic devices [4, 5, 8].

Bistable molecules include (i) singlet-triplet bistable compounds, particularly diradicals, (ii) donor–acceptor complexes, (iii) spin-crossover compounds, (iv) SMMs, (v) *cis–trans* isomers, (vi) *E–Z* isomers, (vii) valence tautomers, and (viii) proton tautomers. Diradical bistability observed in organic molecules, where the energy gap between singlet and triplet states is small, allowing equilibrium between these two spin states [2, 3, 6, 7, 11]. Donor–acceptor complexes exhibit bistability with reversible electron transfer between neutral and ionic states [12]. Spin-crossover compounds, such as Mn(III) Schiff base complexes, undergo transition

Extended author information available on the last page of the article

between low-spin and high-spin states in response to thermal or optical activation [13]. SMMs, including dysprosocenium-based lanthanide complexes, demonstrate bistability between different magnetic states (usually ferromagnetic and antiferromagnetic) through magnetic hysteresis, which arises from slow spin relaxation and high anisotropy [5]. *Cis–trans* isomers, such as cobalt bisphosphine species, have different electronic configurations based on ligand orientation [14]. *E–Z* isomers, exemplified by alkenes and azobenzenes, experience reversible photoisomerization; *E–Z* notation provides a more general way to describe the stereochemistry than the traditional *cis–trans* notation [15]. Valence tautomers, such as cobalt dioxolene systems, exhibit reversible intramolecular redox switching between different oxidation states [16]. Proton tautomers, such as 7-hydroxyquinoline derivatives, endure photoinduced proton transfer between tautomeric forms with different electronic structures [17].

The listed diversity of types of bistable molecules and the variety of applications based on such molecules show the relevance of further searching for new types of molecular bistability. The methods of synthesis of cyclic hydrocarbons have been elaborated [18, 19] (see also [20] for a review). Moreover, cyclic polyaromatic molecules that contain double atomic carbon chains have recently been observed at laser evaporation of carbon nanobelts [21]. Based on these studies, the possibility of synthesizing carbon nanobracelets has recently been proposed [22]. These carbon nanobracelets are cyclic macromolecules with alternating polycyclic regions and double atomic carbon chains. Here, we show that interaction between adjacent chains may lead to a new type of molecular bistability.

In the present paper, we use calculations based on density functional theory (DFT) to predict that the carbon nanobracelets can be bistable molecules. Two states of the bistable nanobracelets are found to have the same topological structure of covalent bonds, but different symmetries and electronic structure. Based on the calculated structural characteristics and electronic properties, we propose that the bistability of the carbon nanobracelets is associated with the competition between the electron structure energy and the energy of interaction between the adjacent chains.

Methods

Structure optimization of carbon nanobracelets was performed using the spin-polarized all-electron DFT calculations with PBE functional [23] implemented in the Priroda code [24]. The molecular geometries were fully optimized without symmetry constraints until the maximum gradient fell below 10^{-4}. The convergence criterion for the self-consistent field (SCF) procedure was set to 10^{-5}. Analytical Hessian matrices were computed in the optimized geometries to verify that the stationary points correspond to true minima (no imaginary frequencies). An integration grid with an accuracy of 10^{-7} was used, ensuring a sufficient precision of numerical integration of the exchange-correlation functional. The optimization was allowed to proceed up to 1000 steps. All calculations were performed in the gas phase using Cartesian coordinates with a singlet spin multiplicity. The singlet ground state has an energy lower than the triplet ground state by approximately 0.2–0.3 eV for all nanobracelets considered [22]. Calculations of carbon nanostructures were also performed in previous works, where it was shown that the stable electronic configuration corresponds to the singlet ground state [25, 26]. This confirms that the singlet description is appropriate for the systems considered here.

Additionally, the optimized geometries were subsequently employed to recompute the dispersion contribution in order to account for long-range interactions that are not captured in standard DFT calculations. This was done using the D3(BJ) dispersion correction with Becke–Johnson damping as proposed by Grimme and co-workers [27, 28].

The spin–orbit coupling (SOC) effect was included in all calculations. In the Priroda code, spin–orbit interaction is taken into account by default within the relativistic framework of the method, ensuring accurate treatment of systems containing heavier elements without requiring additional user-defined parameters. Atomic charges were obtained using the Hirshfeld population analysis, which provides a more physically meaningful and stable description of electronic charge distribution compared to the traditional Mulliken approach, avoiding basis-set-dependent artifacts and ensuring smooth charge variations along molecular geometries and reaction coordinates.

This code allows to considerably reduce the computational time and therefore to study large molecules. The comparison of oxygen adsorption energy on different carbon nanostructures [29] and energetics of interaction between oxygen and small metal clusters [30] with the values obtained using other DFT-based codes gives the adequacy of the Priroda code. Energies of the molecules were calculated taking into account the zero-point energy. The energy-optimized extended Gaussian basis set of triple-n quality of the large component and the corresponding kinetically balanced basis for the small component were used [31].

The Geometry, Frequency, Noncovalent, eXtended Tight Binding (GFN-xTB) method [32] was used to obtain reference geometries, verify the stability of optimized structures, and evaluate intermolecular interaction energies at a semiempirical level of theory. The GFN-xTB calculations were performed using the default accuracy setting (accuracy = 1), corresponding to an integral cutoff of 25.0 bohr, the integral neglect threshold of 10^{-8}, and the SCC convergence criterion of 10^{-6}. These parameters ensure a balanced trade-off between numerical precision and computational efficiency,

as recommended for general-purpose molecular systems in the GFN-xTB methodology. All calculations were performed with these standard thresholds without additional modifications. The method employs a self-consistent tight-binding Hamiltonian with the van der Waals correction D4, multipole electrostatics, and density-dependent repulsion terms.

To investigate the stability of the local minimum corresponding to the high-symmetry state, we performed *ab initio* molecular dynamics (AIMD) simulations for the nanobracelets consisting of 4 and 5 monomers in Orca 6.1 software [33]. All AIMD simulations were performed at the DFT level using the BLYP functional with Grimme's D3 dispersion correction and the def2-SVP basis set. Ten independent trajectories were generated for each molecule, with initial atomic velocities corresponding to 300 K. A Berendsen thermostat was used to maintain the temperature at 300 K with a relaxation time constant of 10 fs. The simulations used a time step of 0.5 fs, and each trajectory was propagated for 2000 steps, corresponding to a total simulation time of 1 ps.

The presence of long flexible carbon atomic chains in the structure of the considered nanobracelets leads to slowing down of the optimization, because the energy changes slightly when the chains bend. The following procedure was used to obtain the starting coordinates for DFT-based optimization close to the minima and thus to decrease computational time. First, hand-made coordinates have been optimized by molecular mechanics [34]. Then, PM3 optimization implemented in MOPAC2016 [35] with and without high-symmetry conservation has been performed to obtain the starting coordinates of the high-symmetry and low-symmetry states of the nanobracelets, respectively. After that, the structure optimization using the Priroda code was performed without applying any symmetry restrictions.

The symmetry of the nanobracelets after optimization of the structure using the Priroda code was determined by the algorithm [36] implemented in the free WebMO server software [37, 38]. All optimized molecules for both stable states have only positive vibrational frequencies. Therefore, the optimized structures of the molecules correspond to the true minima. The lists of coordinates of optimized structures and vibrational frequencies are openly available in *Mendeley Data*, see Ref. [39]. The molecular electrostatic potential is visualized by Jmol [40].

Carbon bistable nanobracelets properties

Previously, the structure, energy, and electronic properties of carbon nanobracelets with 8 carbon atoms in the chains have been studied [22]. The nanobracelets with polycyclic regions with and without hydrogen atoms at the edges and consisting of 1 to 5 monomers were considered. In that study, only nanobracelets with the highest possible symmetry have been found. Here, we consider the carbon nanobracelets with 7 carbon atoms in chains and polycyclic regions without hydrogen atoms at the edge. Here, for nanobracelets consisting of 4 and 5 monomers, bistability with different symmetry of states was discovered. However, only the high-symmetry state is found for the nanobracelets consisting of 2 and 3 monomers using the same optimization procedure. Note that this optimization procedure only gives high-symmetry state for the nanobracelets with 8 atoms in the chains [22] consisting of 1, 2, 3, 4, and 5 monomers, even when starting the optimization from the low-symmetry state.

Structure and energy

The relative energies of the nanobracelets considered per monomer E/n_{m}, where n_{m} is the number of monomers in the nanobracelet, and the radii of the nanobracelet R from the center of mass calculated using the DFT-PBE and GFN2-xTB methods are listed in Table 1. It can be seen that taking into account van der Waals correction leads to qualitatively the same energies for the small nanobracelets without bistability (consisting of 2 and 3 monomers) and to quantitatively similar energies for the nanobracelets with bistability (consisting of 4 and 5 monomers). Calculating the nanobracelet energies taking into account D3 dispersion correction using DFT-optimized coordinates without additional optimization does not lead to noticeable changes in energy (see Table 1). Namely, the energy difference between low-symmetry and high-symmetry states decreases by only 0.4 and 0.3 eV per monomer for the nanobracelets consisting of 4 and 5 monomers, respectively. Note that previous studies also give some evidence in favor of the fact that although DFT-based calculations do not take into account van der Waals interaction, they give adequate values of energy changes at relative displacement of carbon nanoobjects in the case where some overlap of electron density of nanoobjects takes place. For example, DFT-based calculations give the value of the barrier to relative displacement of graphene layers [41, 42] in excellent agreement with the experiment [43], and this result is independent of the use of different corrections for the van der Waals interaction [42]. To compare with previous studies of nanobracelets with 8 atoms in chains [22], all the properties below are discussed for the values obtained by DFT calculations.

The low-symmetry state is found to have lower energy than the high-symmetry state for both nanobracelets with 4 and 5 monomers which have two states. The nearly exponential decrease in relative energy E/n_{m} with increase in n_{m} has previously been found for the high-symmetry nanobracelets with 8 atoms in chains [22]. In contrast, for the high-symmetry state of nanobracelets with 7 atoms in chains, we find that E/n_{m} exhibits a non-monotonic dependence on n_{m}, showing no clear decreasing trend. The radii

Table 1 Structural and electronic properties of the studied nanobracelets with number of monomers n_m from 2 to 5: symmetry after optimization, circumscribed sphere radius (from the center of mass), short and long bond lengths in the chain without terminal bonds connecting to the polycyclic fragment, variation of the bond lengths in the chain δ, energy of the nanobracelet per monomer E/n_m relative to the lowest energy low-symmetry nanobracelet with 4 monomers, dipole moment, HOMO-LUMO energy gap $E_{H\text{-}L}$, the absolute values of HOMO and LUMO energies. Structural parameters and HOMO and LUMO energies are obtained by DFT calculations without the dispersion correction

n_m	Symmetry[a)]	Radius (Å)	Short lengths (Å)	Long lengths (Å)	δ (pm)	E/n_m (eV)			Dipole (D)		$E_{H\text{-}L}$ (eV)		$-E_{HOMO}$ (eV)	$-E_{LUMO}$ (eV)
						DFT	DFT-D3	GFN2-xTB	DFT	GFN2-xTB	DFT	GFN2-xTB		
High-symmetry nanobracelets														
2	D_{2h}	6.52	1.26−1.28	1.30	3.0	0.517	0.419	0.689	0	0	0.566	0.225	5.48	4.92
3	D_{3h}	9.04	1.26−1.28	1.30	3.1	0.197	0.132	0.285	0	0	0.424	0.239	5.36	4.94
4	D_4	11.49	1.25−1.27	1.29−1.31	3.1	0.251	0.209	0.279	0	0	0.136	0.082	5.26	5.13
5	D_{5h}	13.94	1.26−1.28	1.30	3.1	0.238	0.217	0.264	0	0	0.180	0.100	5.31	5.13
Low-symmetry nanobracelets														
4	D_{2d}	11.08	1.26−1.28	1.29−1.30	2.3	0	0	0	0	0	0.397	0.301	5.30	4.91
5	C_2	13.81	1.26−1.28	1.29−1.30	2.2−2.4	0.076	0.085	0.048	0.2	0.1	0.174	0.228	5.25	5.07

[a)] The tolerance with what the symmetry group was detected was ≤ 0.013 for high-symmetry nanobracelets and ≤ 0.03 for low-symmetry nanobracelets

R of the high-symmetry nanobracelets considered linearly depend on the number of monomers $n_m \geq 2$ and behave as $R(n_m) = (1.60 + 2.47n_m)$ Å within the standard deviation 0.03 Å. Note that a linear dependence $R(n_m)$ with the same standard deviation has previously been found for high-symmetry nanobracelets with 8 atoms in chains [22].

To study stability of the high-symmetry state corresponding to the local minimum, AIMD simulations are performed for the nanobracelets consisting of 4 and 5 monomers, with 10 independent trajectories generated for each molecule at temperature 300 K. All observed trajectories correspond to vibrations of atoms near positions corresponding to the local minimum, and no transitions to the ground low-symmetry state or other local minima were observed. Therefore, based on these simulations, it can be expected that both states can coexist at room temperature. This allows applications based on switching between states.

The optimized structures of the states with high and low symmetry for nanobracelets consisting of 4 and 5 monomers are presented in Fig. 1, and all different bond lengths within one monomer are indicated. An alternation of bond length is possible for atomic carbon chains within nanostructures

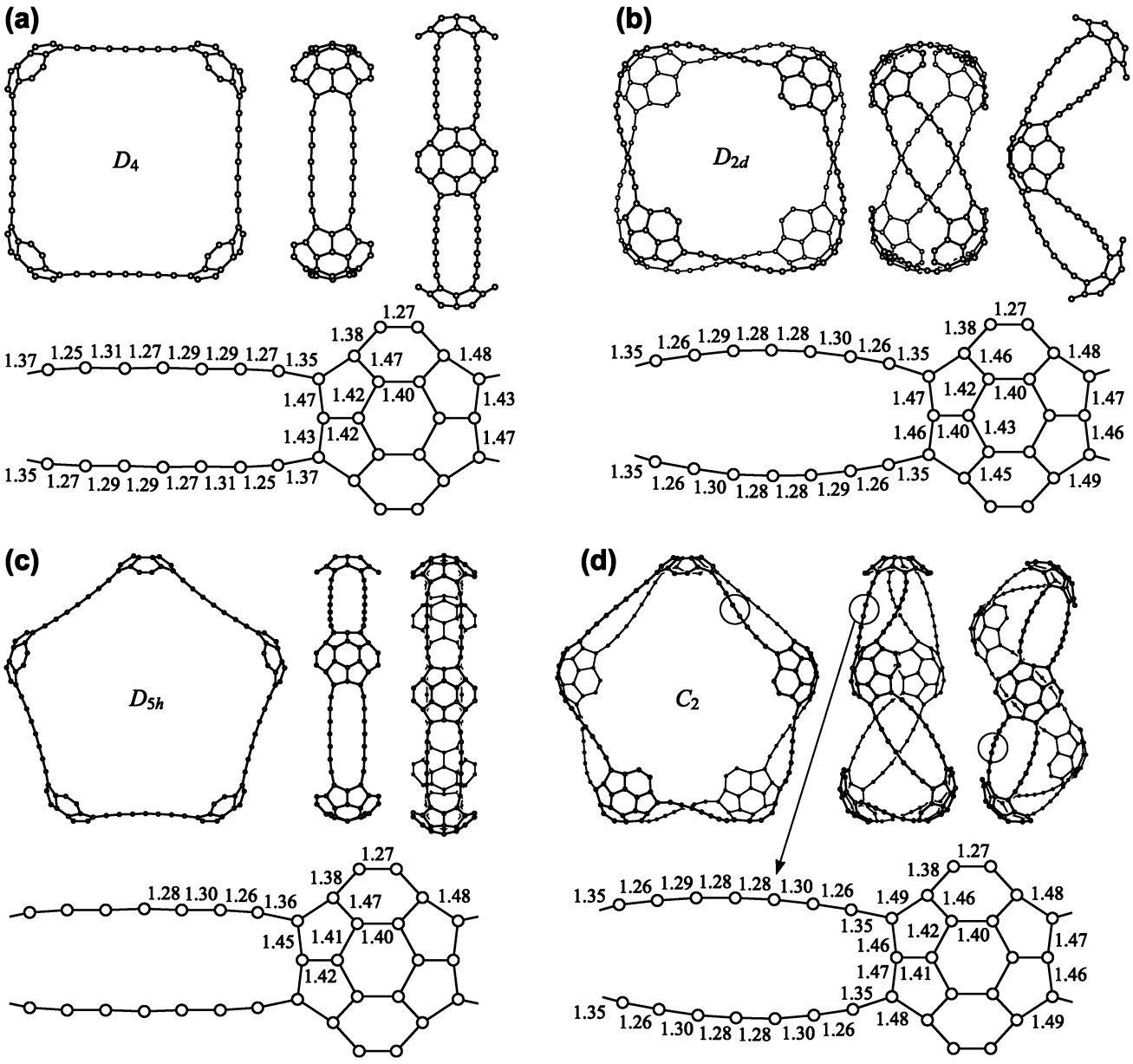

Fig. 1 Carbon nanobracelets composed of $n_m = 4$ monomers (**a**) and (**b**) and of $n_m = 5$ monomers (**c**) and (**d**). There are shown the molecules optimized by DFT-PBE method with high symmetry D_4 (**a**) and D_{5h} (**c**) and with low symmetry D_{2d} (**b**) and C_2 (**d**). Each nanobracelet is shown in three projections. Lengths of nonequivalent bonds are shown in the monomer fragment of the nanobracelet below projections. Monomer fragment in the bottom of panel (**d**) is indicated by red circles in corresponding projections

and molecules [44–50], carbon rings [51–53], and carbon nanotubes [54]. To characterize the alternation of bond length along the chain, the amplitude δ of bond length variations in chains is calculated as follows: [45, 46]

$$\delta = \frac{1}{2}\left|\frac{1}{n_e}\sum_{j=1}^{n_e}(d_{2j-1} + d_{n-(2j-1)}) - \frac{1}{n_0}\sum_{j=1}^{n_0}(d_{2j} + d_{n-2j})\right|, \quad (1)$$

where $d_i = |\vec{r}_i - \vec{r}_{i+1}|$ is the bond length between i-th and $(i+1)$-th atoms in the chain, n is the total number of atoms in the chain, natural numbers $n_e = (n+2)/4$ and $n_0 = n/4$ (the integer part is taken). The terminal bonds connecting the chain to the polycyclic fragment are not taken into account in this equation. The amplitudes of bond length variations are presented in Table 1. According to previous calculations, atomic carbon chains with an even number of atoms (even chains) are polyynes with alternating single and triple bonds –C≡C– [44–50], while odd chains in the middle section are cumulenes with consecutive double bonds =C=C= [44, 46–48, 50]. For the high-symmetry nanobracelets, the following structural characteristics coincide with the results obtained previously for odd carbon chains: (i) the calculated amplitudes δ are consistent with values of 3.0–3.5 pm [46], 2.6–3.1 pm [50], and 2.8–2.9 pm [50] for chains of 9, 11, and 13 atoms, respectively; (ii) the bonding pattern changes from alternation between single and triple bonds at the ends to equal double bonds in the middle of the chain, exhibiting symmetry in bond length distribution relative to the central atom. The chains of the low-symmetry nanobracelets have lower amplitude values $\delta = 2.2$–2.4 pm and lose symmetry relative to the central atom [44, 46, 47]. These structural changes in low-symmetry nanobracelet chains probably occur by decreasing the energy associated with the electronic structure within the chains.

To consider the difference in the interaction between the neighbor chains of the high-symmetry and low-symmetry nanobracelets, the distances between atoms of neighbor chains with the same position in the chains are shown in Fig. 2. These distances for the high-symmetry and low-symmetry nanobracelets are in the ranges 3.2–3.4 Å and 3.3–4.0 Å, respectively. As discussed below, the greater distances between atoms of adjacent chains in low-symmetry nanobracelets lead to a significant reduction in the overlap of electron density of adjacent chains and, hence, to corresponding changes in the interaction energy between chains.

Electronic properties

To reveal possible differences in electronic properties of the low-symmetry and high-symmetry nanobracelets, we calculated the molecular electrostatic potential (related to

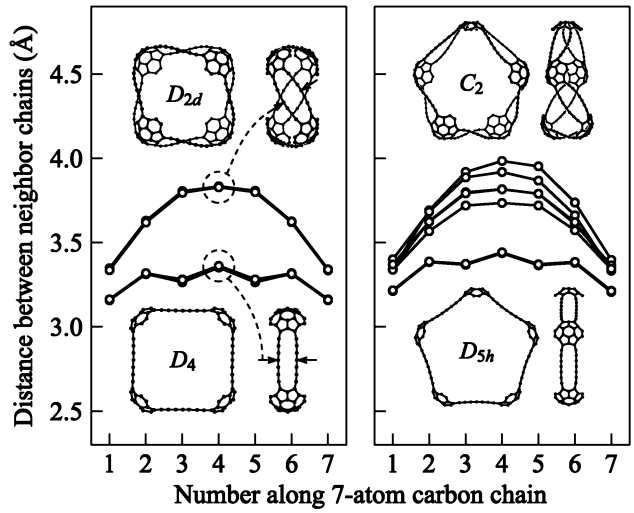

Fig. 2 Distances (in Å) between atoms of adjacent chains with the same position in the chains in high (D_4 and D_{5h}) and low (D_{2d} and C_2) symmetry nanobracelets consisting of 4 and 5 monomers obtained by DFT calculations

atomic charges), the energies and visualizations of the highest occupied molecular orbital (HOMO) and lowest unoccupied molecular orbital (LUMO), as well as the dipole moment. The resulting HOMO and LUMO energies, E_{HOMO} and E_{LUMO}, HOMO-LUMO energy gap, $E_{H\text{-}L}$, and dipole moment for the considered nanobracelets calculated using DFT-PBE and GFN2-xTB methods are listed in Table 1.

Only the low-symmetry nanobracelet consisting of 5 monomers possesses a permanent electric dipole moment, which is allowed by its C_2 symmetry group [55]. In all other cases studied, the calculated dipole moment is zero with an accuracy of 0.01 D. The absence of a dipole moment confirms the assigned symmetry of the nanobracelet states.

The gap $E_{H\text{-}L}$ between the HOMO and LUMO energy levels is an important factor in understanding the stability of the nanobracelet. The values of gap $E_{H\text{-}L}$ for the high-symmetry nanobracelets consisting of 4 and 5 monomers, for which the bistability is found, 0.136 and 0.180 eV, respectively, are several times lower than for high-symmetry nanobracelets with 2 and 3 monomers without the bistability (see Table 1). Note that the values of gap $E_{H\text{-}L}$ for all the considered high-symmetry nanobracelets with 8 atoms in chains are greater 0.27 eV, and all these nanobracelets are without the bistability [22]. This suggests a possible correlation between the gap $E_{H\text{-}L}$ and the bistability of the nanobracelets. The considerable difference between the values of gap for the high-symmetry nanobracelets with an even ($E_{H\text{-}L} = 0.276$–0.279 eV) and odd ($E_{H\text{-}L} = 0.500$–0.629 eV) number of monomers with 8 atoms in chains has been previously found [22]. Such an evident difference in the gap for even and odd numbers n_m is not observed here for the nanobracelets with 7 atoms in chains. Both calculation methods yield a

considerable increase in the gap $E_{H\text{-}L}$ due to the symmetry breaking for the nanobracelet consisting of 4 monomers, while for the nanobracelet consisting of 5 monomers, this gap $E_{H\text{-}L}$ increase is obtained only by the GFN2-xTB method. This behavior may be related to the Jahn–Teller-type effect, where orbital degeneracy in a high-symmetry state leads to spontaneous break of symmetry and stabilization of a low-symmetry state, accompanied by an increase in the gap $E_{H\text{-}L}$.

The molecular electrostatic potential is calculated using $\sum_A Z_A/r_A$, where Z_A is the partial charge on an atom A calculated by the Priroda code (in units of the elementary charge e) and r_A is the distance from an atom A to a particular point on the isosurface. This potential characterizes the interaction energy of a positive point unit charge (i.e., a proton) with the atomic charges. To show the interaction between adjacent chains, the isosurface is taken at the van der Waals distance of 1.95 Å from the atoms of a nanobracelet (see Fig. 3). Some overlap of the isosurfaces of neighbor chains at the van der Waals distance for the high-symmetry nanobracelets means an overlap of electron clouds. Therefore, very weak covalent-like bonds between the neighbor chains can exist. For the low-symmetry nanobracelets, the symmetry breaking leads to an increase of the distance between neighbor chains, so that the overlap of electron clouds is absent in the middle part of neighbor chains, with no possibility of weak covalent bonds between chains. Additionally, increasing the distance between adjacent chains results in a decrease in van der Waals attraction between the chains. Both of these effects reduce the contribution of the interaction energy between the chains to the total binding energy of the nanobracelet. Thus, it is probable that the minimum of the interaction energy between the chains corresponds to the high-symmetry state. On the other hand, the opposite effect can also exist. Since the chains are negatively charged, the adjacent chains repel each other. Therefore, the breaking of symmetry with a decrease in the distance between adjacent chains results in a decrease in Coulomb repulsion between the chains and, consequently, in a decrease in positive Coulomb term in the interaction energy between chains.

By examining the plots of molecular orbitals, one can qualitatively assess the degree of π-electron delocalization within the structure of nanobracelets (see Fig. 4). In the high-symmetry nanobracelets, the π-orbitals in chains exhibit extended delocalization, forming continuous isosurfaces between pairs of adjacent carbon atoms. These orbital shapes resemble "tubes" that connect the atoms, indicat-

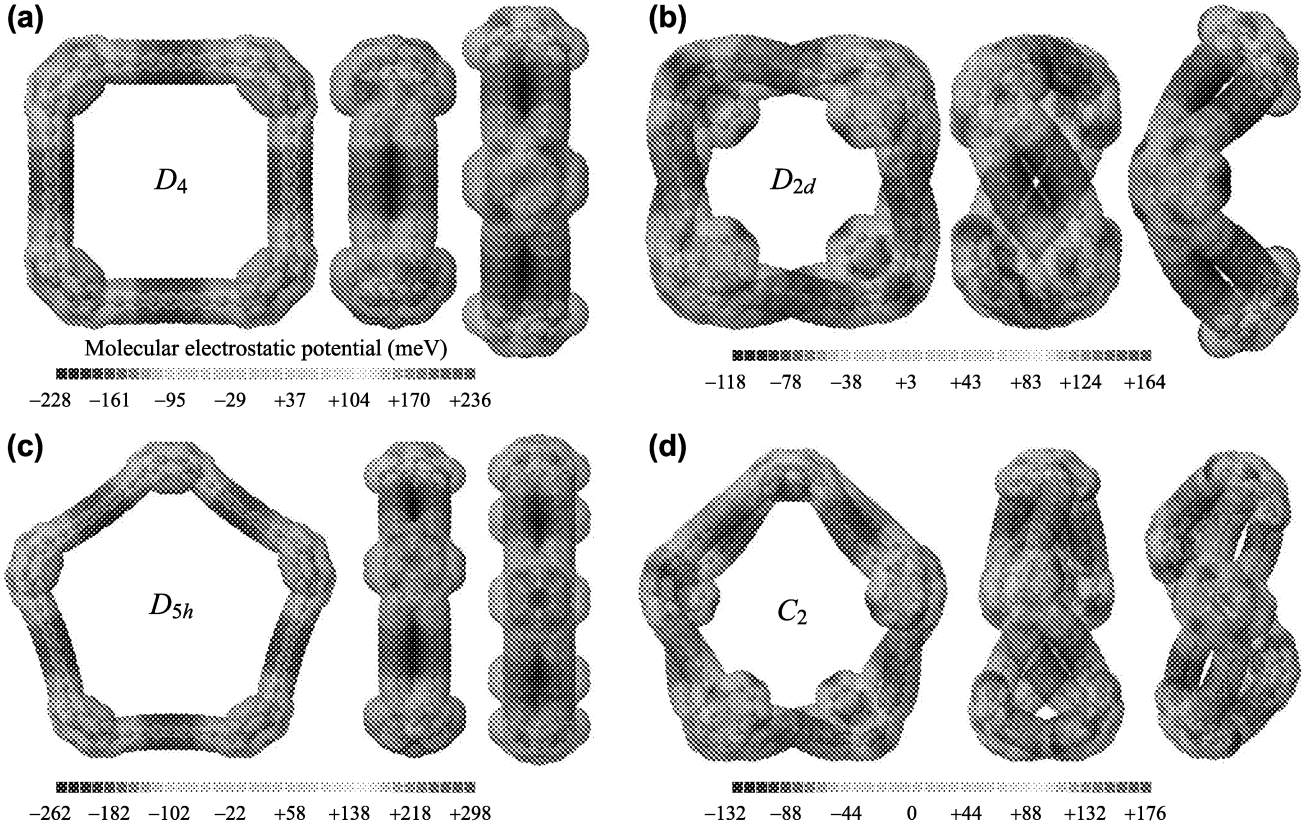

Fig. 3 Molecular electrostatic potential (MEP; in millielectronvolts) at the distance 1.95 Å from atoms of the molecule obtained by DFT calculations. Sign of MEP corresponds to the sign of atomic charge. The nanobracelet states and projections in (**a**)–(**d**) are identical to those in Fig. 1

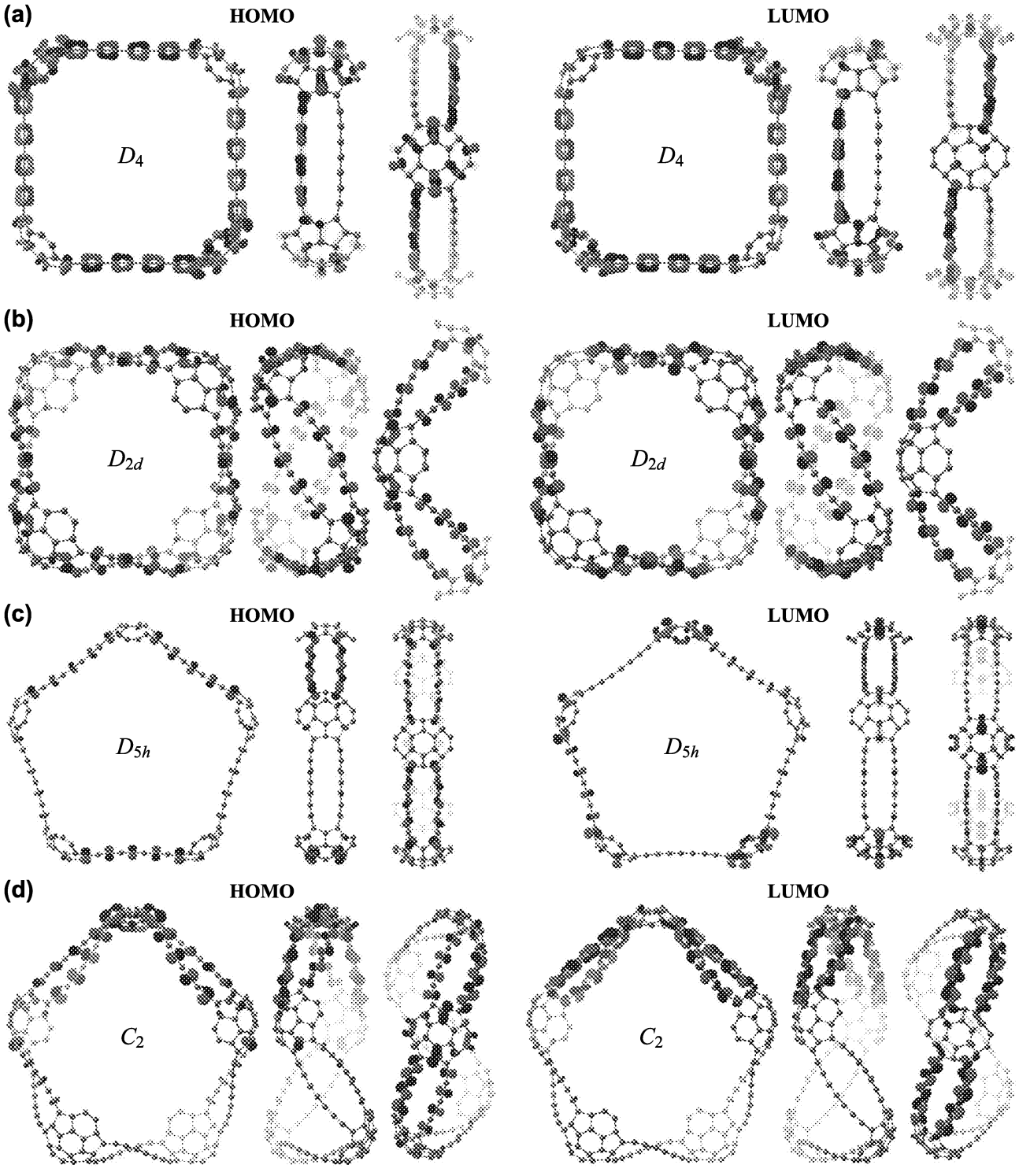

Fig. 4 Visualizations of HOMO and LUMO (highest occupied molecular orbital and lowest unoccupied molecular orbital) for nanobracelets. The nanobracelet states and projections in (**a**)–(**d**) are identical to those in Fig. 1

ing effective conjugation throughout the cyclic molecule. In contrast, the low-symmetry nanobracelets demonstrate partial localization of the π-system, with orbitals appearing more isolated and localized to individual atomic sites. The breaking of symmetry leads to disrupted conjugation and the formation of localized orbital lobes that resemble atomic p-orbitals. This transition from the delocalized to the localized orbital structure in the low-symmetry nanobracelets suggests

a decrease in π-overlap. Since ordinary carbon chains with an even number of atoms are polyynes with alternating single and triple bonds [44–50], such a decrease in π-overlap can lead to an increase in the related energy of the electronic structure. This makes the low-symmetry state somewhat less favorable in energy. Note that this effect is opposite to the conclusion about the stability of the low-symmetry state based on the analysis of the HOMO-LUMO gap $E_{\text{H-L}}$. In general, the electronic structure becomes more complex as the size of the nanobracelet increases. The HOMO and LUMO visualizations for the nanobracelets composed of 5 monomers also show the change in the electronic structure when the symmetry is broken.

Cause of bistability

Let us now discuss the cause of the found bistability of carbon nanobracelets based on the calculated structural characteristics and electronic properties described above. The bistability means the presence of two minima in dependence of a total energy of a molecule on atom coordinates. For the nanobracelets considered, the total energy consists of two contributions: the energy associated with the electronic structure and the energy associated with the interaction between adjacent chains, with different dependences on the coordinates of the atoms. The analysis of the HOMO-LUMO gaps leads to the conclusion that the low-symmetry state corresponds to the minimum of the energy associated with the electronic structure. However, the analysis of the HOMO-LUMO visualizations allows us to assume that the low-symmetry state is somewhat less favorable in energy. Some overlap of electron density between adjacent chains is present in the high-symmetry state and absent in the low-symmetry state. This overlap may indicate the existence of very weak covalent bonds between the adjacent chains in the high-symmetry state. In this case, the minimum interaction energy of the adjacent chains corresponds to the high-symmetry state. The van der Waals attraction between the adjacent chains also contributes to the minimum of the total energy corresponding to the high-symmetry state, while Coulomb repulsion between chains has the opposite effect. In any case, we believe that the presence of two stable states is associated with competition between the energy of interaction between the chains and the electron structure energy.

Conclusions and discussion

Our DFT calculations reveal bistability in carbon nanobracelets (cyclic macromolecules with alternating polycyclic regions bridged by 7-atom double carbon chains), showing the existence of two distinct stable states with low and high symmetry. These states have the same topological structure of covalent bonds but different symmetry and electronic structure. In contrast, previous studies of pure carbon molecules addressed only topology-switching transitions (ring-to-star isomerization of the C_{10} molecule) [56]. Note that DFT calculations give two possible states for carbon rings: with alternating bond lengths and equal angles between bonds and opposite with equal bond lengths and alternating angles between bonds [51–53]. However, bistability has not been found for carbon rings, since for a ring of a given size, only one stable state is possible, while the other state is unstable [53].

The bistability is caused by the interplay of two energies: the electron structure energy within the nanobracelet and the energy associated with interaction between the adjacent chains. We believe that the low-symmetry state, which is the ground state of the nanobracelet, corresponds to the minimum of the electron structure energy. The high-symmetry state corresponds probably to the minimum of energy of interaction between the adjacent chains. This minimum is associated with the formation of very weak covalent bonds between the chains. The total energy of the high-symmetry state is 1.0 and 0.8 eV higher for nanobracelets with 4 and 5 monomers, respectively. By analogy, the revealed type of bistability may exist in other nanostructures and macromolecules that contain double atomic carbon chains. We believe that this study will stimulate further research on molecules and nanostructures exhibiting such bistability and their applications.

Acknowledgements Y.G.P. and A.M.P. acknowledge the support by the Russian Science Foundation grant no. 23-42-10010, https://rscf.ru/en/project/23-42-10010/. S.A.V., S.V.R., and N.A.P. acknowledge support by the Belarusian Republican Foundation for Fundamental Research (grant no. F23RNF-049) and by the Belarusian National Research Program "Convergence-2030".

Author Contributions Sergey A. Vyrko: investigation, methodology, visualization, writing—review and editing.
Yulia G. Polynskaya: investigation, writing—original draft.
Nikita A. Matsokin: investigation, visualization, writing—original draft.
Andrey M. Popov: conceptualization, funding acquisition, investigation, project administration, writing—original draft.
Andrey A. Knizhnik: investigation, methodology, software.
Sergey V. Ratkevich: investigation, methodology.
Nikolai A. Poklonski: funding acquisition, investigation, project administration, supervision, writing—review and editing.

Data Availability The raw data that support the findings of this study are openly available in Mendeley Data at https://doi.org/10.17632/454j49xbv3, see Ref. [39].

Declarations

Conflict of interest The authors declare no competing interests.

References

1. Costa P, Lohmiller T, Trosien I, Savitsky A, Lubitz W, Fernandez-Oliva M, Sanchez-Garcia E, Sander W (2016) Light and temperature control of the spin state of bis(*p*-methoxyphenyl)carbene: a magnetically bistable carbene. J Am Chem Soc 138(5):1622–1629. https://doi.org/10.1021/jacs.5b11696
2. Catarina G, Turco E, Krane N, Bommert M, Ortega-Guerrero A, Gröning O, Ruffieux P, Fasel R, Pignedoli CA (2024) Conformational tuning of magnetic interactions in coupled nanographenes. Nano Lett 24(40):12536–12544. https://doi.org/10.1021/acs.nanolett.4c03518
3. Shimizu A, Morikoshi T, Sugisaki K, Shiomi D, Sato K, Takui T, Shintani R (2022) Synthesis and isolation of a Kekulé hydrocarbon with a triplet ground state. Angew Chem Int Ed 61(29):e202205729. https://doi.org/10.1002/anie.202205729
4. Urdampilleta M, Ayela C, Ducrot PH, Rosario-Amorin D, Mondal A, Rouzières M, Dechambenoit P, Mathonière C, Mathieu F, Dufour I, Clérac R (2018) Molecule-based microelectromechanical sensors Sci Rep 8:8016. https://doi.org/10.1038/s41598-018-26076-2
5. Goodwin CAP, Ortu F, Reta D, Chilton NF, Mills DP (2017) Molecular magnetic hysteresis at 60 kelvin in dysprosocenium. Nature 548(7668):439–442. https://doi.org/10.1038/nature23447
6. Zhou W, Fei Y, Zhang YS, Miao X, Jiang SD, Liu J (2025) Triplet-ground-state nonalternant nanographene with high stability and long spin lifetimes. Nat Commun 16:1006. https://doi.org/10.1038/s41467-024-54276-0
7. Mishra S, Vilas-Varela M, Lieske LA, Ortiz R, Fatayer S, Rončević I, Albrecht F, Frederiksen T, Peña D, Gross L (2024) Bistability between π-diradical open-shell and closed-shell states in indeno[1,2-*a*]fluorene. Nat Chem 16(5):755–761. https://doi.org/10.1038/s41557-023-01431-7
8. Liu J, Chen YC, Liu JL, Vieru V, Ungur L, Jia JH, Chibotaru LF, Lan Y, Wernsdorfer W, Gao S, Chen XM, Tong ML (2016) A stable pentagonal bipyramidal Dy(III) single-ion magnet with a record magnetization reversal barrier over 1000 K. J Am Chem Soc 138(16):5441–5450. https://doi.org/10.1021/jacs.6b02638
9. Canton SE, Biednov M, Pápai M, Lima FA, Choi TK, Otte F, Jiang Y, Frankenberger P, Knoll M, Zalden P, Gawelda W, Rahaman A, Møller KB, Milne C, Gosztola DJ, Zheng K, Retegan M, Khakhulin D (2023) Ultrafast Jahn-Teller photoswitching in cobalt single-ion magnets. Adv Sci 10(21):2206880. https://doi.org/10.1002/advs.202206880
10. Zanella S, Aragon-Alberti M, Brite CDS, Salles F, Carlos LD, Long J (2023) Luminescent single-molecule magnets as dual magneto-optical molecular thermometers. Angew Chem Int Ed 62(35):e202306970. https://doi.org/10.1002/anie.202306970
11. Toews R, Köhn A (2024) Cyclohepta[def]fluorene as a bistable molecule: first principles studies on its electronic structure and the effects of benzo-extension, substitution and solvation. Phys Chem Chem Phys 26(30):20462–20469. https://doi.org/10.1039/D4CP02247E
12. Rumble CA, Vauthey E (2019) Structural dynamics of an excited donor-acceptor complex from ultrafast polarized infrared spectroscopy, molecular dynamics simulations, and quantum chemical calculations. Phys Chem Chem Phys 21(22):11797–11809. https://doi.org/10.1039/C9CP00795D
13. Kühne IA, Ozarowski A, Sultan A, Esien K, Carter AB, Wix P, Casey A, Heerah-Booluck M, Keene TD, Müller-Bunz H, Felton S, Hill S, Morgan GG (2022) Homochiral Mn^{3+} spin-crossover complexes: a structural and spectroscopic study. Inorg Chem 61(8):3458–3471. https://doi.org/10.1021/acs.inorgchem.1c03379
14. Wang JY, Ruan ZY, Kong H, Deng W, Wu SG, Liu JL, Tong ML (2025) Low-/high-spin cobaltaboratranes stabilized by *cis*-/*trans*-isomeric bisphosphines. Inorg Chem 64(19):9842–9851. https://doi.org/10.1021/acs.inorgchem.5c01152
15. Kistemaker JCM, Pizzolato SF, van Leeuwen T, Pijper TC, Feringa BL (2016) Spectroscopic and theoretical identification of two thermal isomerization pathways for bistable chiral overcrowded alkenes. Chem Eur J 22(38):13478–13487. https://doi.org/10.1002/chem.201602276
16. Glotz G, Knaipp K, Maier MS, Hüll K, Novak A, Kelterer AM, Griebenow T, Herges R, Trauner D, Gescheidt G (2023) To isomerize or not to isomerize? *E*/*Z* isomers of cyclic azobenzene derivatives and their reactivity upon one-electron reduction. Chem Eur J 29(35):e202300146. https://doi.org/10.1002/chem.202300146
17. Lapinski L, Rostkowska H, Nowacki J, Nowak MJ (2023) Photoinduced long-distance hydrogen-atom transfer in molecules with a 7-hydroxyquinoline frame and a carbaldehyde or aldoxime group as the intramolecular hydrogen transporting crane. J Phys Chem A 127(14):3104–3113. https://doi.org/10.1021/acs.jpca.3c00170
18. Jasti R, Bhattacharjee J, Neaton JB, Bertozzi CR (2008) Synthesis, characterization, and theory of [9]-, [12]-, and [18]cycloparaphenylene: carbon nanohoop structures. J Am Chem Soc 130(52):17646–17647. https://doi.org/10.1021/ja807126u
19. Povie G, Segawa Y, Nishihara T, Miyauchi Y, Itami K (2017) Synthesis of a carbon nanobelt. Science 356(6334):172–175. https://doi.org/10.1126/science.aam8158
20. Segawa Y, Yagi A, Matsui K, Itami K (2016) Design and synthesis of carbon nanotube segments. Angew Chem Int Ed 55(17):5136–5158. https://doi.org/10.1002/anie.201508384
21. Tanuma Y, Dunk P, Maekawa T, Ewels CP (2022) Chain formation during hydrogen loss and reconstruction in carbon nanobelts. Nanomaterials 12(12):2073. https://doi.org/10.3390/nano12122073
22. Vyrko SA, Polynskaya YG, Matsokin NA, Popov AM, Knizhnik AA, Poklonski NA, Lozovik YE (2024) Carbon nanobracelets. Chem Phys Lett 835:140999. https://doi.org/10.1016/j.cplett.2023.140999
23. Perdew JP, Burke K, Ernzerhof M (1996) Generalized gradient approximation made simple. Phys Rev Lett 77(18):3865–3868. https://doi.org/10.1103/PhysRevLett.77.3865
24. Laikov DN, Ustynyuk YA (2005) PRIRODA-04: a quantum chemical program suite. New possibilities in the study of molecular systems with the application of parallel computing. Russ Chem Bull Int Ed 54(3):820–826. https://doi.org/10.1007/s11172-005-0329-x
25. Aryanpour K, Mazumdar S, Zhao H (2012) Triplet excitations in carbon nanostructures. Phys Rev B 85:085438. https://doi.org/10.1103/PhysRevB.85.085438
26. Tretiak S (2007) Triplet state absorption in carbon nanotubes: a TD-DFT study. Nano Lett 7(8):2201–2206. https://doi.org/10.1021/nl070355h
27. Grimme S, Antony J, Ehrlich S, Krieg H (2010) A consistent and accurate *ab initio* parametrization of density functional dispersion correction (DFT-D) for the 94 elements H-Pu. J Chem Phys 132(15):154104. https://doi.org/10.1063/1.3382344
28. Grimme S, Ehrlich S, Goerigk L (2011) Effect of the damping function in dispersion corrected density functional theory. J Comput Chem 32(7):1456–1465. https://doi.org/10.1002/jcc.21759
29. Polynskaya YG, Matsokin NA, Sinitsa AS, Knizhnik AA, Potapkin BV (2022) First-principles investigation of interaction between the atomic oxygen species and carbon nanostructures. Carbon Trends 9:100201. https://doi.org/10.1016/j.cartre.2022.100201
30. Pichugina DA, Polynskaya YG, Kuz'menko NE (2016) Spin and structural features of oxygen dissociation on tetrahedral Ag_{20} and

$Ag_{19}Au$ clusters. Phys Chem Chem Phys 18(27):18033–18044. https://doi.org/10.1039/c6cp01630h
31. Laikov DN (2005) A new class of atomic basis functions for accurate electronic structure calculations of molecules. Chem Phys Lett 416(1–3):116–120. https://doi.org/10.1016/j.cplett.2005.09.046
32. Bannwarth C, Ehlert S, Grimme S (2019) GFN2-xTB–an accurate and broadly parametrized self-consistent tight-binding quantum chemical method with multipole electrostatics and density-dependent dispersion contributions. J Chem Theory Comput 15(3):1652–1671. https://doi.org/10.1021/acs.jctc.8b01176
33. Neese F (2011) The ORCA program system. WIREs Comput Mol Sci 2(1):73–78. https://doi.org/10.1002/wcms.81
34. Allinger NL (1977) Conformational analysis. 130. MM2. A hydrocarbon force field utilizing V_1 and V_2 torsional terms. J Am Chem Soc 99(25):8127–8134. https://doi.org/10.1021/ja00467a001
35. Stewart JJP (1989) Optimization of parameters for semiempirical methods II. Applications J Comput Chem 10(2):221–264. https://doi.org/10.1002/jcc.540100209
36. Largent RJ, Polik WF, Schmidt JR (2012) Symmetrizer: algorithmic determination of point groups in nearly symmetric molecules. J Comput Chem 33(19):1637–1642. https://doi.org/10.1002/jcc.22995
37. WebMO: web-based interface for computational chemistry programs. https://www.webmo.net/demoserver/. Accessed 12 September 2025
38. Polik WF, Schmidt JR (2021) WebMO: web-based computational chemistry calculations in education and research. WIREs Comput Mol Sci 12(1):e1554. https://doi.org/10.1002/wcms.1554
39. Vyrko SA, Polynskaya YG, Matsokin NA, Popov AM, Knizhnik AA, Ratkevich SV, Poklonski NA (2025) Data for: Bistable carbon nanobracelets. Mendeley Data. https://doi.org/10.17632/454j49xbv3
40. Jmol development team (2021-05-29) Jmol v. 14.31.41. http://jmol.sourceforge.net/
41. Lebedeva IV, Knizhnik AA, Popov AM, Lozovik YE, Potapkin BV (2011) Interlayer interaction and relative vibrations of bilayer graphene. Phys Chem Chem Phys 13(13):5687–5695. https://doi.org/10.1039/c0cp02614j
42. Lebedeva IV, Lebedev AV, Popov AM, Knizhnik AA (2017) Comparison of performance of van der Waals-corrected exchange-correlation functionals for interlayer interaction in graphene and hexagonal boron nitride. Comput Mater Sci 128:45–58. https://doi.org/10.1016/j.commatsci.2016.11.011
43. Alden JS, Tsen AW, Huang PY, Hovden R, Brown L, Park J, Muller DA, McEuen PL (2013) Strain solitons and topological defects in bilayer graphene. PNAS 110(28):11256–11260. https://doi.org/10.1073/pnas.1309394110
44. Khoo KH, Neaton JB, Son YW, Cohen ML, Louie SG (2008) Negative differential resistance in carbon atomic wire-carbon nanotube junctions. Nano Lett 8(9):2900–2905. https://doi.org/10.1021/nl8017143
45. Ravagnan L, Manini N, Cinquanta E, Onida G, Sangalli D, Motta C, Devetta M, Bordoni A, Piseri P, Milani P (2009) Effect of axial torsion on *sp* carbon atomic wires. Phys Rev Lett 102:245502. https://doi.org/10.1103/PhysRevLett.102.245502
46. Zanolli Z, Onida G, Charlier JC (2010) Quantum spin transport in carbon chains. ACS Nano 4(9):5174–5180. https://doi.org/10.1021/nn100712q
47. Cahangirov S, Topsakal M, Ciraci S (2010) Long-range interactions in carbon atomic chains. Phys Rev B 82:195444. https://doi.org/10.1103/PhysRevB.82.195444
48. Zhou Y, Li Y, Li J, Dong J, Li H (2017) Electronic transport properties of carbon and boron nitride chain heterojunctions. J Mater Chem C 5(5):1165–1178. https://doi.org/10.1039/C6TC04936B
49. Sinitsa AS, Lebedeva IV, Polynskaya YG, de Oteyza DG, Ratkevich SV, Knizhnik AA, Popov AM, Poklonski NA, Lozovik YE (2021) Transformation of a graphene nanoribbon into a hybrid 1D nanoobject with alternating double chains and polycyclic regions. Phys Chem Chem Phys 23(1):425–441. https://doi.org/10.1039/d0cp04090h
50. Lebedeva IV, Vyrko SA, Sinitsa AS, Ratkevich SV, Popov AM, Knizhnik AA, Poklonski NA, Lozovik YE (2024) Magnetic and electronic properties of 1D hybrid nanoobjects composed of alternating polycyclic hydrocarbon regions and double carbon chains. Comput Theor Chem 1241:114913. https://doi.org/10.1016/j.comptc.2024.114913
51. Martin JML, El-Yazal J, François JP (1995) Structure and vibrational spectra of carbon clusters C_n (n = 2-10, 12, 14, 16, 18) using density functional theory including exact exchange contributions. Chem Phys Lett 242(6):570–579. https://doi.org/10.1016/0009-2614(95)00801-A
52. Martin JML, Taylor PR (1996) Structure and vibrations of small carbon clusters from coupled-cluster calculations. J Phys Chem 100(15):6047–6056. https://doi.org/10.1021/jp952471r
53. Torelli T, Mitas L (2000) Electron correlation in C_{4N+2} carbon rings: aromatic versus dimerized structures. Phys Rev Lett 85(8):1702–1705. https://doi.org/10.1103/PhysRevLett.85.1702
54. Poklonski NA, Ratkevich SV, Vyrko SA, Kislyakov EF, Bubel' ON, Popov AM, Lozovik YE, Hieu NN, Viet NA (2012) Structural phase transition and band gap of uniaxially deformed (6,0) carbon nanotube. Chem Phys Lett 545(Suppl. C):71–77. https://doi.org/10.1016/j.cplett.2012.07.023
55. Atkins P, de Paula J, Keeler J (2023) Atkins' Physical Chemistry. Oxford University Press Oxford. https://doi.org/10.1201/b12795
56. Poklonski NA, Ratkevich SV, Vyrko SA (2015) Quantum-chemical calculation of carbododecahedron formation in carbon plasma. J Phys Chem A 119(34):9133–9139. https://doi.org/10.1021/acs.jpca.5b03573

Authors and Affiliations

Sergey A. Vyrko[1] · Yulia G. Polynskaya[2] · Nikita A. Matsokin[2] · Andrey M. Popov[3] · Andrey A. Knizhnik[2] · Sergey V. Ratkevich[1] · Nikolai A. Poklonski[1]

✉ Nikolai A. Poklonski
poklonski@bsu.by

Sergey A. Vyrko
vyrkosergey@tut.by

Yulia G. Polynskaya
yupol@kintechlabs.com

Nikita A. Matsokin
nikita@matsokin.ru

Andrey M. Popov
popov-isan@mail.ru

Andrey A. Knizhnik
knizhnik@kintechlabs.com

Sergey V. Ratkevich
ratkevich@bsu.by

1 Physics Department, Belarusian State University, Nezavisimosti Ave. 4, Minsk 220030, Belarus

2 Kintech Lab Ltd., 3rd Khoroshevskaya Street 12, Moscow 123298, Russia

3 Institute of Spectroscopy Russian Academy of Science, Fizicheskaya Str. 5, Troitsk Moscow 108840, Russia